ELSEVIER

Contents lists available at ScienceDirect

Earth and Planetary Science Letters

www.elsevier.com/locate/epsl



A stable isotope record of late Cenozoic surface uplift of southern Alaska



Nicholas S. Bill ^{a,b,*,1}, Hari T. Mix ^{c,1}, Peter U. Clark ^a, Sean P. Reilly ^c, Britta J.L. Jensen ^{d,e}, Jeffrey A. Benowitz ^f

- ^a College of Earth, Ocean, and Atmospheric Sciences, Oregon State University, Corvallis, OR 97331, USA
- ^b Institute of Earth Sciences, University of Iceland, Reykjavík 101, Iceland
- ^c Department of Environmental Studies and Sciences, Santa Clara University, Santa Clara, CA 95053, USA
- ^d Department of Earth and Atmospheric Sciences, University of Alberta, Edmonton, Alberta T6G 2E3, Canada
- e Royal Alberta Museum, Edmonton, Alberta, T5N 0M6, Canada
- ^f Geophysical Institute, University of Alaska Fairbanks, Fairbanks, AK 99775, USA

ARTICLE INFO

Article history: Received 26 December 2016 Received in revised form 6 November 2017 Accepted 12 November 2017 Available online 24 November 2017 Editor: H. Stoll

Keywords: Alaska surface uplift stable isotopes paleoenvironmental change hydrologic cycle paleoaltimetry

ABSTRACT

Although the timing of an acceleration in late-Cenozoic exhumation of southern Alaska is reasonably well constrained as beginning $\sim 5-\sim 6$ Ma, the surface uplift history of this region remains poorly understood. To assess the extent of surface uplift relative to rapid exhumation, we developed a stable isotope record using the hydrogen isotope composition (δD) of paleo-meteoric water over the last ~ 7 Ma from interior basins of Alaska and Yukon Territory. Our record, which is derived from authigenic clays (δD_{clay}) in silicic tephras, documents a $\sim 50-60\%$ increase in δD values from the late Miocene ($\sim 6-\sim 7$ Ma) through the Plio-Pleistocene transition ($\sim 2-\sim 3$ Ma), followed by near-constant values over at least the last ~ 2 Ma. Although this enrichment trend is opposite that of a Rayleigh distillation model typically associated with surface uplift, we suggest that it is consistent with indirect effects of surface uplift on interior Alaska, including changes in aridity, moisture source, and seasonality of moisture. We conclude that the δD_{clay} record documents the creation of a topographic barrier and the associated changes to the climate of interior Alaska and Yukon Territory.

© 2017 Elsevier B.V. All rights reserved.

1. Introduction

Earth's topography reflects the dynamic balance of the feedbacks among tectonic and Earth-surface processes and climate (England and Molnar, 1990). As such, determining paleo-elevation and paleoclimate histories of mountain belts provides insight into interactions of these processes and their contribution to the evolution of surface topography (Chamberlain et al., 2012; Chase et al., 1998; Feng et al., 2016, 2013; Feng and Poulsen, 2016; Insel et al., 2012; Mix et al., 2011; Mulch and Chamberlain, 2007; Pavlis et al., 1997; Poulsen et al., 2010; Rowley and Garzione, 2007).

Southern Alaska is one of the most tectonically active region's in the world, as evidenced by dramatic topographic relief that forms the Earth's highest coastal mountain range, with peaks rising from sea level to over 6-km elevation over relatively short

distances (O'Sullivan et al., 1997). Recent work has provided clear evidence that feedbacks between tectonics and erosion associated with collision of the Yakutat terrane have contributed directly to rapid exhumation of this region over the last few million years (Berger et al., 2008; Enkelmann et al., 2010; McAleer et al., 2009; Meigs et al., 2008). Active tectonics is expressed by high seismicity and continental convergence rates of 40-55 mm yr⁻¹ (Savage and Plafker, 1991). Precipitation rates of up to 7 myr^{-1} in the coastal mountains support widespread coverage of the mountains by glaciers and ice fields with corresponding high mass fluxes, resulting in some of the highest rates of glacial erosion on Earth (Hallet et al., 1996; Sheaf et al., 2003). Finally, thermochronology reveals rapid exhumation and rock uplift of coastal (St. Elias-Chugach Mountain Range) and interior (Wrangell Mountains, Alaska Range) mountain ranges during the late Cenozoic (Benowitz et al., 2013, 2012, 2011; Berger et al., 2008; Enkelmann et al., 2010; Fitzgerald et al., 1995, 1993; McAleer et al., 2009; Meigs et al., 2008; Plafker et al., 1992; Riccio et al., 2014) (Fig. 1).

Collision and subduction of the Yakutat terrane began ~ 30 Ma, but an acceleration in rates of exhumation and rock uplift $\sim 5 \sim 6$ Ma (Fig. 1) is generally attributed to a change in the direc-

^{*} Corresponding author at: Institute of Earth Sciences, University of Iceland, Reyk-javík 101, Iceland.

E-mail address: nbill@hi.is (N.S. Bill).

¹ These authors contributed equally to this work.

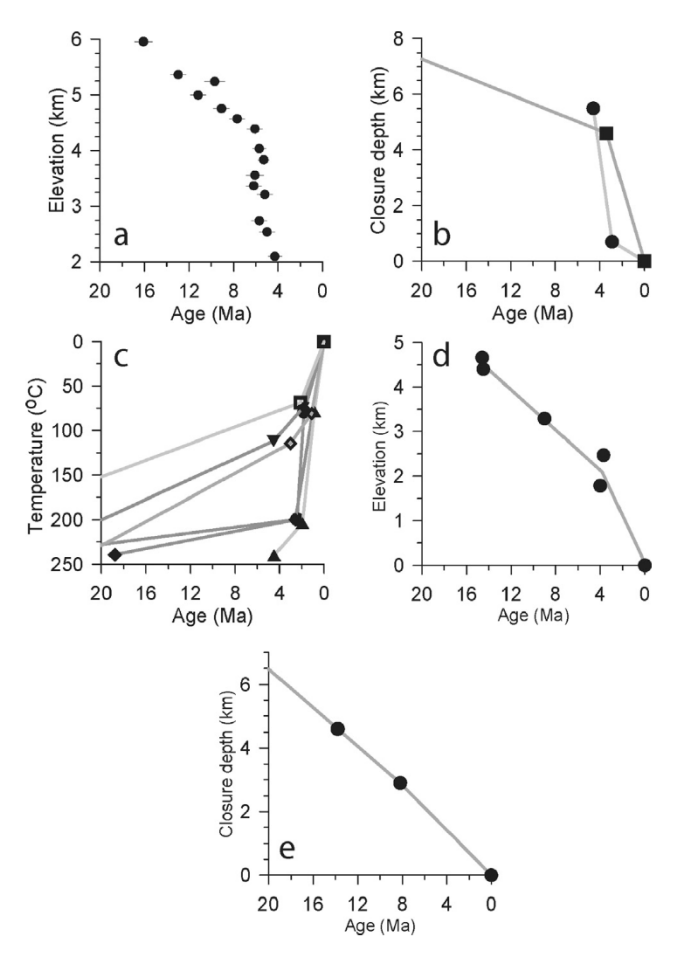


Fig. 1. Thermochronology data constraining rock uplift and exhumation over last 20 Myr for several areas of Alaska. Panels a-d show an acceleration over last 5-6 Myr from several Alaska ranges, whereas panel e shows constant values from the Chugach terrane, which is representative of the stable North American upper plate in more interior Alaska. (a) Variation of apatite fission-track age with elevation from central Alaskan Range (Fitzgerald et al., 1995). (b) Apatite and zircon thermochronology data constraining closure depth from the Yakutat terrane (Meigs et al., 2008). (c) Apatite and zircon helium and fission track ages constraining time-temperature paths for Mt. Fairweather region (McAleer et al., 2009). (d) Variation of apatite fission-track age with elevation from Mt. Logan (O'Sullivan and Currie, 1996). (e) Apatite and zircon thermochronology data constraining closure depth from the Chugach terrane (North American upper plate) (Meigs et al., 2008).

tion of plate movement from NW to NNW accompanied by an increase in the rate of plate convergence (Benowitz et al., 2013; Fitzgerald et al., 1995; Lease et al., 2016; Plafker et al., 1992; Trop and Ridgway, 2007). The resulting increase in oblique collision and in the rate of underthrusting led to an increase in sedimentation rates in regional basins as well as increased exhumation and rock uplift of the Saint Elias and Chugach Mountains, the Alaska Range, and adjacent regions (Bruhn et al., 2004; Enkelmann et al., 2010; Fitzgerald et al., 1995, 1993; Little and Naeser, 1989; Pavlis et al., 2012, 2004; Plafker et al., 1994; Ridgway et al., 2007).

While records of increased exhumation and sedimentation provide clear signals of increased rock uplift and erosion of the Alaskan ranges $\sim\!5\text{--}6$ Ma, evidence for the lateral extent of surface uplift and its timing to produce the present-day orography remains uncertain, requiring additional constraints to establish the temporal relation between collision, exhumation, and surface uplift. Here we develop a $\sim\!\!7$ Ma stable isotope record of paleo-precipitation from sites that are leeward of coastal and interior Alaskan mountain ranges to evaluate whether there is a signal of increasing surface uplift that accompanied the acceleration in exhumation beginning $\sim\!\!5\!-\!\sim\!\!6$ Ma.

Stable isotope records provide one of the few methods of reconstructing the surface-uplift history of the world's mountains by exploiting systematic changes in the δD or $\delta^{18}O$ values of meteoric water that ultimately can be related to changes in paleoenvironment and paleoelevation (Blisniuk and Stern, 2005; Feng et al., 2016, 2013; Galewsky et al., 2016; Mulch, 2016; Rowley and Garzione, 2007; Stern et al., 1997). This technique has been used to reconstruct past elevation histories of the Himalayas and Tibetan Plateau (Garzione et al., 2000; Gebelin et al., 2013; Rowley et al., 2001; Rowley and Currie, 2006), the Andes (Canavan et al., 2014; Garzione et al., 2008; Ghosh et al., 2006; Mulch et al., 2010; Stern and Blisniuk, 2002), the New Zealand Southern Alps (Chamberlain et al., 1999), the European Alps (Campani et al., 2012) and western North America (Poage and Chamberlain, 2002; Takeuchi and Larson, 2005; Sjostrom et al., 2006; Mulch and Chamberlain, 2007; Mix et al., 2011; Chamberlain et al., 2012). As the coastal and interior mountain ranges in Alaska provide a strong orographic barrier to onshore moisture transport today (Fig. 2), we expect the dominant control on water isotope ratios of modern precipitation in interior Alaska to be continentality. We thus expect that changes in the δD of paleo-precipitation from interior Alaska would be strongly influenced by surface uplift-dependent changes in continentality and the hydrologic cycle.

2. Existing evidence of regional surface uplift

Several lines of evidence suggest that the regional extent of surface uplift of the Alaskan ranges increased during the late Miocene and Pliocene, and thus may have accompanied the acceleration in exhumation and rock uplift beginning $\sim 5-\sim 6$ Ma. We note where uncertainties in understanding exist, specifically, that direct elevation estimates are absent. What we outline below are changes in surficial geological features that can oftentimes be explained by processes other than surface uplift. In many cases, the resolution of the dating constraints is too low to resolve whether the surface uplift was contemporaneous with the acceleration in exhumation over the last $\sim 5-\sim 6$ Ma.

2.1. Paleogeographic reconstructions

There has been recent work using detrital geochronology to constrain the Miocene paleo-drainage reorganization history across interior Alaska. Brennan and Ridgway (2015) applied detrital U-Pb zircon source to sink analysis to the paleo-Tanana Basin as a proxy for major changes in sediment source with time. They constrained a change from dominantly north of the Alaska Range sediment sourcing changing to dominantly intra-Alaska Range and south of the Alaska Range by ~15 Ma and inferred surface uplift was underway by this time. Davis et al. (2015) applied detrital $^{40}\mathrm{Ar}/^{39}\mathrm{Ar}$ source to sink analysis to the same paleo-Tanana Basin strata as a proxy for major changes in sediment source with time. They constrained a change from dominantly north of the Alaska Range sediment sourcing changing to dominantly intra-Alaska Range and south of the Alaska Range by ~20 Ma and inferred surface uplift was underway by this time. Both these studies are in agreement with regional thermochronology studies demonstrating rock uplift in the Alaska Range was underway by ~30 Ma (Benowitz et al., 2013, 2012, 2011; Burkett et al., 2015; Fitzgerald et al., 2014; Haeussler et al., 2008; Lease et al., 2016; Riccio et al., 2014). None of this previous research studies puts constraints on when the Alaska Range was laterally extensive enough to be an orographic barrier.

North of the central Alaska Range, the Neogene (\sim 23- \sim 2.6 Ma) Tanana basin contains a sedimentary record of the collision of the Yakutat terrane. Based on paleocurrents and clast composition of conglomerates, Wahrhaftig et al. (1969) showed that

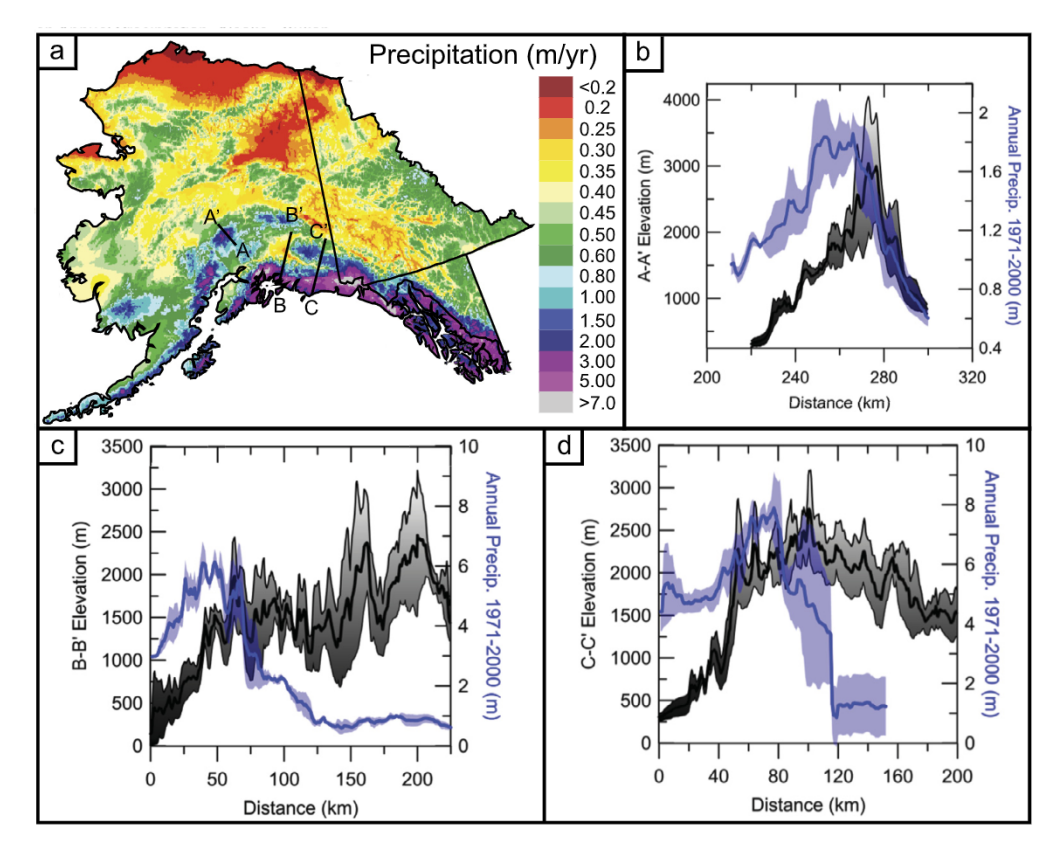


Fig. 2. Overview of topography and modern precipitation of the Alaska/Yukon region. All climate data shown in panels $\mathbf{a-d}$ are from PRISM gridded climate estimates using 1971–2000 average climatologies at a resolution of 2.5-arc minutes (\sim 3 km²), interpolated from observational precipitation data at 544 weather stations (www.prism.oregonstate.edu). (\mathbf{a}) Mean annual precipitation of the Alaska/Yukon region. The color bar on right indicates annual precipitation amounts on map in m/yr. ($\mathbf{b-d}$) Representative transects shown on panel \mathbf{a} . For each transect, a mean (solid line) and standard deviation (2σ shaded uncertainty band) was derived from multiple transects at regular intervals in the transect area. (\mathbf{b}) Alaska Range (A-A' transect) mean precipitation (blue) and mean elevation (black). (\mathbf{c}) Chugach through Wrangell mountains (B-B' transect) mean precipitation (blue) and mean elevation (black). (For interpretation of the references to color in this figure legend, the reader is referred to the web version of this article.)

sediments of the late-Miocene Grubstake Formation record dominantly southward-flowing fluvial systems transporting sediment from the Yukon-Tanana terrane to the north. These sediments are unconformably overlain by the Pliocene Nenana Gravel, which records northward-flowing fluvial systems draining the central Alaska Range from the south, suggesting a drainage reversal as the range underwent surface uplift. Ridgway et al. (2007) reinterpreted these provenance changes as indicating an increase in sediment contribution from sources located south of the basin associated with northward propagation of thrust sheets toward the southern margin of the Tanana basin. Moreover, they documented source changes in the Nenana Gravel that are consistent with progressive northward exhumation of plutons located south of the Pliocene Tanana basin. Both interpretations invoke a change in basin fill source to the Tanana basin that began during the late Miocene as a result of a flexural response to northward propagation of shortening within the central Alaska Range, and is thus consistent with onset of an increase in extent of surface elevation.

2.2. Increase in glaciation

Glacial-marine deposits of the Yakataga Formation provide evidence for nearly continuous glaciation of the Chugach/St. Elias Range since at least \sim 5.6 Ma, which has been interpreted as requiring surface uplift of the Alaskan coastal ranges to intersect the equilibrium line altitude (ELA) to support glaciers (Eyles et al., 1991; Lagoe et al., 1993). The history of large valley glaciation in the Alaska Range is not well constrained, but by \sim 3 Ma glacially derived loess was accumulating in interior Alaska (Westgate et al., 1990). There is a documented glacial erosion related increase in

exhumations rates in the Alaska Range at this time (Benowitz et al., 2011; Lease et al., 2016) implying topography must have been tall enough to sustain glacial growth.

2.3. Uplifted volcanics

Volcanic rocks of the St. Clare Creek volcanic field were erupted between $\sim 18-\sim 11$ Ma onto a low-relief surface prior to uplift of the Saint Elias Mountains (Skulski et al., 1992; Souther and Stanciu, 1975). The northern part of the field has been intensely folded, which appears to have been concentrated in the Pliocene-Pleistocene (O'Sullivan and Currie, 1996), with folded lava beds suggesting substantial crustal thickening and an order of 2 km of surface uplift (Souther and Stanciu, 1975).

2.4. Paleoenvironmental reconstructions

White et al. (1997) reconstructed paleoenvironments of the last \sim 18 Ma for areas extending from north of the Alaska Ranges to the Arctic Ocean. Low-resolution and poorly dated palynological records indicate that after \sim 7 Ma, there was an increase in aridity and continentality. White et al. (1997) attributed this to a combination of global cooling and the surface uplift of the Alaska Range and St. Elias Mountains, which were thought to have reduced the transport of warm, moist Pacific air masses to the Alaskan interior. Péwé et al. (2009) using stable isotope analysis (δ^{13} C), flora, fossils, and palynology demonstrated by at least \sim 2 Ma interior Alaska had a similar continental dry-cold climate as present day. The question remains when did the topography of the Alaska Range reach a lateral and vertical extent great enough to change the climate of interior of Alaska.

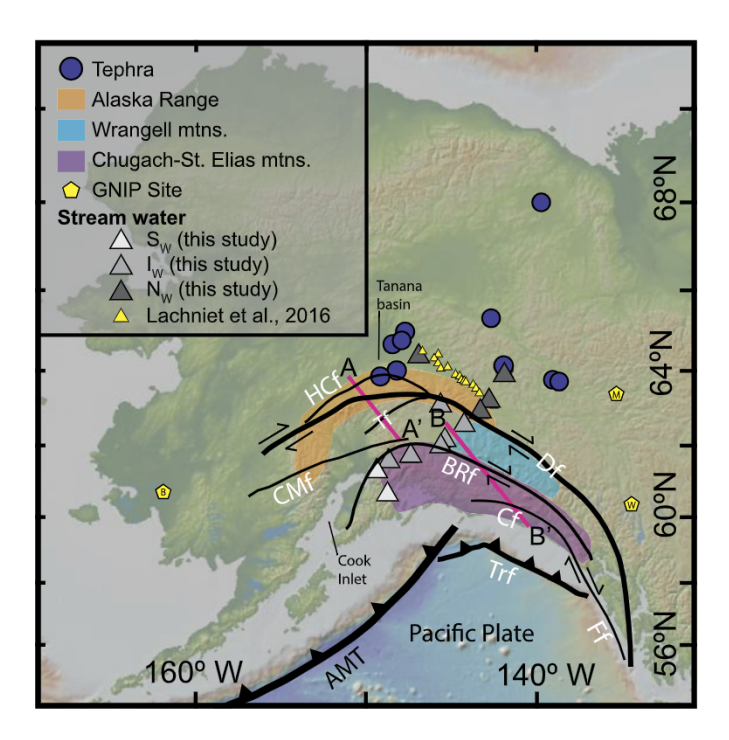


Fig. 3. Overview map of the field area and generalized tectonics of Alaska, The abbreviation of fault names are as follows: BRf: Border Ranges fault system, Trf: Transition fault, CMf: Castle Mountain fault, Df: Denali fault, Tf: Talkeetna fault, Ff: Fairweather fault, Cf: Chugach fault, HCf: Hines Creek fault, AMT: Aleutian Mega-Thrust. Orange shading represents the Alaska Range complex, blue shading shows the Wrangell Mountains complex, and purple shading shows the Chugach-St. Elias fold-and-thrust belt complex. Triangles represent stream water isotope analyses. The gray triangles are measured surface water from our analysis, where the data are divided into three groups: Sw = south of all topography, Iw = Intermediate between coastal and interior topography, N_w = Leeward of all topography. Yellow triangles are stream water samples from Lachniet et al. (2016) that are leeward of all topography and geographically contained by our N_w samples. Yellow pentagons show locations of the GNIP sites: M = Mayo, Yukon Territory, and W = Whitehorse, Yukon Territory. Blue circles show field locations of tephras analyzed for this study. The pink transect lines denote the two general transects used in the composite geologic cross section in Fig. 5. Some symbols may be indicative of more than one sample location but only one symbol can be shown due to symbol size. Base map is from the Global Multi-Resolution Topography (GMRT) synthesis (www.geomapapp.org) (Ryan et al., 2009). (For interpretation of the references to color in this figure legend, the reader is referred to the web version of this article.)

3. Methods

3.1. Modern water samples

In order to provide a framework for assessing topographic influences on the isotopic composition of paleo-meteoric water, we collected surface waters for δD and $\delta^{18}O$ analyses along a transect from the coast to the interior of Alaska (Fig. 3). We divide our water samples into three groups: samples along the coast, windward of all coastal mountain ranges (S_W, n=2); samples from the lee of the coastal mountain ranges, but windward of the more interior Alaska Range (I_W, n=6); samples that are leeward (north) of all ranges (N_W, n=4) (Fig. 4).

We sampled stream water from small catchments between August–September 2014. This approach provides time-integrated and spatially resolved patterns of the isotopic composition of precipitation and near-surface groundwater, thus reducing bias from short-term, daily to seasonal meteorological variations and from downstream mixing of waters from larger catchments that incorporate significantly different isotopic regimes (Kendall and Coplen, 2001; Schemmel et al., 2013).

Samples were collected as unfiltered water in 125 mL Nalgene polyethylene bottles, with as little air volume as possible in the

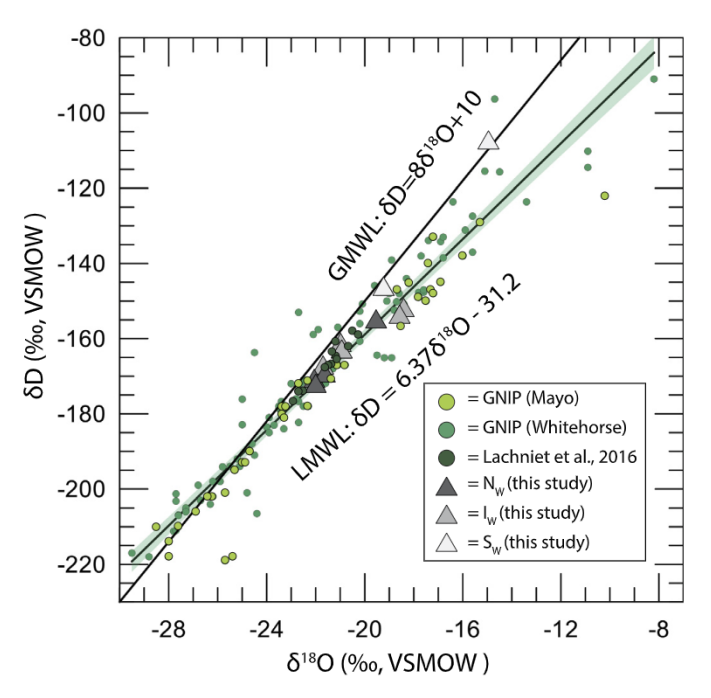


Fig. 4. Modern surface water isotope data and local meteoric water line (LMWL) calculated for the interior of Alaska. The LMWL is calculated as a linear fit of the combined datasets of GNIP (Mayo), GNIP (Whitehorse), Lachniet et al. (2016) and N_W as identified in the legend. The equation of the LMWL is $\delta D = 6.37 \delta^{18} O - 31.2$ ($R^2 = 0.93$), and the green shading shows the LMWL 2σ uncertainty envelope. The global meteoric water line (GMWL) is shown for reference. Error bars are not shown for individual isotope ratio measurements because they are either not provided or smaller than the symbol size.

closed bottles. After collection, the bottle closure was wrapped in parafilm and kept at room temperature and out of sunlight during transport and storage to minimize evaporation. Stable isotopes were measured using a Los Gatos Research off-axis integrated cavity output spectroscopy TWIA-45EP water isotope analyzer. Triplicate measurements of six measured injections were made per sample, with three preparatory injections between measurements to minimize memory effects. δD and $\delta^{18}O$ values were corrected using internal and external reference water standards and are reported relative to VSMOW. We report the average and 2σ for each water sample (Table 1).

3.2. Tephra samples

Stable isotope paleoaltimetry studies typically target geologic archives that capture the signal of past meteoric water during or shortly after the time of deposition. These archives include authigenic clay that weathers from feldspar minerals in volcanic ash, hydrated glass shards from volcanic ash, pedogenic carbonate nodules from paleosols, and carbonate from lacustrine sediments. Deposition in the Alaskan interior basins has occurred since the Miocene (Duk-Rodkin et al., 2004; Trop and Ridgway, 2007), but secondary carbonates are largely absent from these basins due to climate conditions that are unsuitable for carbonate precipitation. On the other hand, they contain abundant, well-dated silicic ashes with feldspars that rapidly weather to authigenic clay minerals in the shallow subsurface (Preece et al., 2011; Westgate et al., 1990). These clay minerals incorporate and preserve the isotopic signal of the meteoric water into their crystal structure, bound in the OH⁻ group (Lawrence and Taylor, 1971), making them ideal paleoclimate and paleoaltimetry proxies (Delgado and Reyes, 1996; Mix and Chamberlain, 2014; Mulch and Chamberlain, 2007; Sjostrom et al., 2006; Tabor and Montañez, 2005; Yapp, 2008).

We collected samples of volcanic tephra from several depositional basins in Alaska and Yukon (Fig. 3). Our tephra samples,

Table 1Modern stream water sample information and stable isotope results.

Water sample number	LAT	LONG	Location name	Description	Elevation (masl)	δD	δD 2σ	$\delta^{18}O$	δ^{18} O 2 σ
AK14-WS1 ^a	64.4752	-146,9751	Munsons Slough	Large Stream	190	-155.0	0.8	-19.50	0.56
AK14-WS2 ^a	64.0714	-141.9338	Chicken Creek	Small Stream	505	-169.4	0.9	-21.62	0.76
AK14-WS3 ^a	63.3255	-142.8366	Tok River	Small River	498	-170.7	1.8	-22.02	0.92
AK14-WS4 ^a	63.0451	-143.3694	Little Tok River	Small River	623	-171.5	0.8	-22.00	0.86
AK14-WS5	62.7163	-144.2426	Unamed Creek	Small Stream	753	-163.2	0.9	-20.92	0.74
AK14-WS6	62,2646	-145.4114	No Name Creek	Small Stream	453	-151.9	0.9	-18.43	0.60
AK14-WS7	63,2295	-145.6285	McCallum Creek	Small River	943	-161.0	1.4	-20.99	0.94
AK14-WS8	62.1093	-145.5589	Moose Creek	Large Stream	431	-153.7	1.0	-18.58	0.88
AK14-WS9	61.8168	-147.4681	Glacial Fan Creek	Small Stream	914	-167.6	1.1	-21.70	0.98
AK14-WS10	61.7318	-148.7493	Kings River	Small River	180	-154.4	0.9	-10.19	0.76
AK14-WS11	61.4509	-149.3760	Eklutna River	Small River	19	-146.5	0.5	-19.15	0.54
AK14-WS12	60.7757	-148.7246	Portage Creek	Small Stream	0	-107.5	1.0	-14.94	0.34

a North of topography.

Table 2 Individual tephra sample information and stable isotope results. The n = values refer to the total number of clay δD analyses that make up each bin, shown as blue circles in Fig. 4 and is the value used to calculate the standard error (SE). We refer the reader to Table S1 for results of the individual analyses.

Age bin (Ma)	Tephra name	Sample ID	LAT	LONG	Age (Ma)	1σ (Ma)	δD	δD SE	n =
0.0-0.5	LC2	AK14-6	64,0707	-141.9158	~ 0.01	_	-102.6	1.9	16
	VT	AK14-18	64.7088	-148.5028	0.106	0.01			
	Halfway House	AK14-23	64.7088	-148.5028	\sim 0.115	-			
	Old Crow	AK14-10	64.7088	-148.5028	0.124	0.01			
	Chester Bluff	UT1744	65.3629	-142.6736	0.243	0.023			
	Stampede	AK14-15	63.8881	-149.1023	~ 0.3	-			
0.5-1.0	GI	AK14-19	64,8586	-147.8529	0.5	0.1	-104.0	4.4	9
	Gold Run	UT1907	63.7470	-138.6960	0.735	0.088			
	SP	AK14-9	64,8553	-147.9306	0.86	0.06			
1.0-1.5	Midnight Dome	UT1495	63.8210	-139.0330	1.09	0.18	-105.5	5.7	8
	Little Timber	UT622	68.0600	-139.7700	1.37	0.12			
	Paradise Hill	UT1556	63,8210	-139.0330	1.5	0.13			
1.5-2.5	PA	AK14-8	64.8553	-147.9306	1.89	0.2	-103.3	3.5	5
	Little Blanche Creek	UT1623	63.8210	-139.0330	\sim 2.5	-			
2.5-3.5	LC3	AK14-20/22	64.0707	-141.9158	~ 3	_	-126.6	8.2	8
	Dago Hill	UT1553	63,8210	-139.0330	3.18	0.41	120.0	0.2	
5.0-6.0	UMG	AK14-2	64.0784	-148.2092	~ 5.0	_	-125.1	3.4	5
	UG	AK14-2 AK14-3	64.0784	-148,2092 -148,2092	~ 5.8	_	-125.1	5.4	3
6.5–7.5	Grubstake	AK14-1/16	64.0784	-148,2092	6.7	0.1	-169.0	3.4	6

all of which are radiometrically dated or closely bracketed by radiometric ages, were collected from the late Miocene–Pliocene Grubstake Formation, the late-Pliocene White Channel Gravel, and Quaternary loess outcrops that collectively span the interval from \sim 6.7 Ma to \sim 0.11 Ma (Table 2 and Supplementary Material – see details on tephra age control). In all cases, the tephra ages and their association with these stratigraphic units are consistent with the regional stratigraphy (Wahrhaftig et al., 1969; Naeser et al., 1982; Ager, 1994; Ager et al., 1994; Triplehorn et al., 2000; Froese et al., 2003; Ridgway et al., 2007; Grimaldi and Triplehorn, 2008; Preece et al., 2011).

We isolated the authigenic clay for their δD composition (δD_{clay}) by disaggregating and suspending each tephra sample in deionized water. The suspended material was centrifuged to leave only the <2- μ m equivalent (clay-size) particles in suspension (Stern et al., 1997). We then dried the supernatant in preparation for stable isotope analysis.

For isotopic analysis, we enclosed clay isolates in silver foil capsules, and then placed them in a Fisher Scientific Isotemp vacuum oven at 80 °C and -100 kPa pressure for at least three days before isotopic analysis. Oven drying the samples removes interstitial water and ensures targeting of the bound OH $^-$ groups that represent the isotopic signal of paleo-meteoric water from the time of clay

formation (Lawrence and Taylor, 1971). Stable isotopes were measured at the Stable Isotope Biogeochemistry Laboratory at Stanford University following the procedures of Mix and Chamberlain (2014), Sharp (1990) and Takeuchi and Larson (2005). δD analyses were obtained through continuous flow mass spectrometry using a thermal combustion elemental analyzer and a Thermo Finnigan DeltaPlusXL mass spectrometer. Samples were analyzed in triplicate along with PEF1 and NBS-22 international reference standard materials in order to constrain the error to less than 2‰.

We combined our dated tephras into bins to account for the resolution of our stable isotope record whereby binning the data accounts for the disproportionate number of younger tephras compared to older ones by placing equal weight on each time bin rather than weighted by total number of analyses (0.5-Myr bins from 0–1.5 Ma and 1.0-Myr bins from 1.5–7.5 Ma). This binning procedure also allows measurements from separate tephras of similar ages to be combined into a single value, which is useful for understanding change over time. Since the age uncertainties on the individual tephras are smaller than the age range of the bin itself, we consider this binning procedure an appropriate technique to report measurements from multiple samples as a single value. Table S1 shows the results for individual isotope ratio measurements, and Table 2 shows the bin intervals, mean δD_{clay} and standard

error for each bin, as well as the number of samples in the population (n =) that fall within each bin.

3.3. Clay mineralogy constraints and assumptions

Clay minerals fractionate hydrogen isotopes differently during their formation (Lawrence and Taylor, 1971), with large differences in mineral-water fractionation depending on mineral species. We were unable to successfully characterize clay mineralogy with X-ray diffraction (XRD) determinations of our samples due to their small size. However, we explicitly assume that our samples are smectite because existing XRD data on clays weathered from Alaskan tephras suggest that clay mineralogy changes from dominantly kaolinite in the early Miocene Healy Creek Formation (> \sim 22 Ma) to dominantly montmorillonite (smectite group) in the middle Miocene Suntrana Formation (<~16 Ma) and all subsequent younger units (Dickson, 1981; Triplehorn, 1976). We rule out conversion to illite because our samples, being collected from unconsolidated surface sediments (largely loess), neither show evidence of recrystallization associated with deep burial nor of hydrothermal alteration. In the following, we identify several robust observational and theoretical constraints that make it highly unlikely that if there are any variations in clay mineralogy and cation chemistry, they do not significantly influence our δD_{clav} signal and corresponding paleoclimate reconstruction.

We first performed sensitivity analyses assessing the degree to which changes in mineralogy or cation chemistry of smectites would affect mineral-water fractionation factors (Tables S2 and S3). At a range of temperatures appropriate for Late-Cenozoic Alaska, differences between the mineral-water fractionation of kaolinite vs. smectite/illite are on the order of 30%. Thus, roughly 60% of the observed 50% increase in δ^{18} O increase could be accommodated by a shift from smectite mineralogy to kaolinite with decreasing age. Kaolin group minerals, however, typically form in warm, humid environments and are therefore unlikely to increase in abundance during the progressively cooling Late Cenozoic, nor in the increasingly seasonal rain shadow environment of interior Alaska (Deepthy and Balakrishnan, 2005). Variations in the octahedral layer chemistry of 2:1 phyllosillicates can also affect mineralwater fractionation. Savin and Lee (1988) and Tabor and Montañez (2005) used a bond-model approach to calibrate smectite-water fractionation by incorporating the mole fractions of Al, Fe and Mg in the octahedral layer. The Tabor and Montañez (2005) fractionation factor was defined as: $1000 \ln(\alpha) = -2.2 * 106/T2 - 7.7 +$ (2XAI - 4XMg - 68XFe) where X is the mole fraction in the octahedral layer. This indicates that Al and Mg variations are relatively small contributors to changing the apparent fractionation, while Fe concentration can produce large (up to 68% for 100% Fe versus 0% Fe) changes in apparent fractionation. A compilation of published smectites and example bond model calculations (Table S3) confirms this theory in practice, as mineral-water fractionation factors from montmorillonites and bentonites are relatively similar, while Fe-rich weathering crusts and notronites can differ by as much as 60%. As noted above, however, existing XRD data on clays weathered from Alaskan tephras from Miocene and younger units is primarily montmorillonite (Dickson, 1981; Triplehorn, 1976) formed by weathering from felsic to intermediate tephras in the shallow subsurface, which is a relatively Fe-poor member of the smectite group. Fe-rich smectites, such as nontronites, typically form as weathering products of basaltic rocks or in hydrothermal settings (Bischoff, 1972). Major element geochemical data from a subset of our samples confirms that they are Fe- and Mg-poor, with Al consisting of 88% of cations on average (Table S4) and we assume that the remainder of our samples have a similar chemistry. Therefore, we rule out the possibility of systematic changes in the octahedral chemistry to drive the large-scale Late Cenozoic δD_{clay} changes documented here.

Finally, we attempted to evaluate the relationships between our δD_{clav} record and our modern surface water δD transect. Using the Capuano (1992) and Tabor and Montañez (2005) fractionation factors, we reconstructed stream water δD values from δD_{clav} values from our δD_{clav} values. In both cases, the reconstructed values are 70 to 100% greater than our modern stream water δD values. This offset is far too large to be accommodated by small changes in mean annual temperature and probably even larger effects such as D-enrichment of surface waters due to evaporation, and likely points to a systematic error in the calibration of δD fractionation for clay minerals. In order to investigate this offset further, we compiled $\delta^{18}O$ and δD compositions from a large number of smectite and kaolinite studies from western North America (Tables S5 and S6) (Mix et al., 2016; Mix and Chamberlain, 2014). Using the appropriate fractionation factor depending on mineralogy and mean annual temperature estimates from paleofloral assemblages (Wolfe et al., 1998), we compared the reconstructed water isotope compositions with that of modern meteoric waters (Bowen, 2017). The offset between reconstructed and measured δD values from these existing clay mineral studies ranged from 23 to 59% (mean of 44‰) while the offset for δ^{18} O ranged from -1.9 to 3.2% (mean of 0.5%). Since the δ^{18} O values accurately reflect the chemistry of meteoric waters, the large discrepancies between observed and reconstructed waters using δD fractionation factors are unlikely due to kinetic fractionation. Instead, we suggest that this is an artifact of δD fractionation factors being obtained from a geopressurized environment (e.g., Capuano, 1992) and therefore may not be appropriate for the near-surface environments required for accurate paleoclimate reconstruction. Therefore, while we refrain from comparing our δD_{clay} record to modern values, comparison of existing δ^{18} O and δ D reconstructions adds robustness to our argument that our δD_{clav} record reliably records paleoclimate trends in Late Cenozoic Alaska.

4. Stable isotope results

4.1. Water samples

Fig. 4 shows modern surface water isotope data from sites leeward of the major mountain ranges of southern Alaska. These data include our water-sample transect data as well as data from two Global Network of Isotopes in Precipitation (GNIP) stations (Mayo and Whitehorse, Yukon) and relevant data from Lachniet et al. (2016). The GNIP data were obtained from the International Atomic Energy Agency (http://www.iaea.org/water). In order to make the Lachniet et al. (2016) data comparable to our transect, we only plot samples within the geographic boundaries of our collected transect and fully leeward of topography (identified in Fig. 3).

The Global Meteoric Water Line (GMWL), representative of equilibrium fractionation, is defined as $\delta D = 8\delta^{18}O + 10$ (Craig, 1961). Today, there is a depletion of water isotopic ratios in a transect from windward to leeward of topography, reflecting the orographic rainout of precipitation moving to the interior of Alaska (Dansgaard, 1964). This is confirmed by the findings of Lachniet et al. (2016) and also suggests that most moisture loss is associated with the more coastal Chugach, Wrangell and St. Elias Ranges (Fig. 2). With this in mind, the windward (S_W) samples plotted on Fig. 4 fall on the GMWL. In contrast, our leeward I_W and N_W data fall off of the GMWL, again consistent with Lachniet et al. (2016).

Using data only from the interior, leeward of all southern Alaska topography, we calculate a Local Meteoric Water Line (LMWL) for the interior of Alaska (Fig. 4) ($\delta D = 6.37\delta^{18}O - 31.2$, $R^2 = 0.93$) by applying a linear fit through the combined datasets of the Whitehorse GNIP data, the Mayo GNIP data, our N_W data, and the

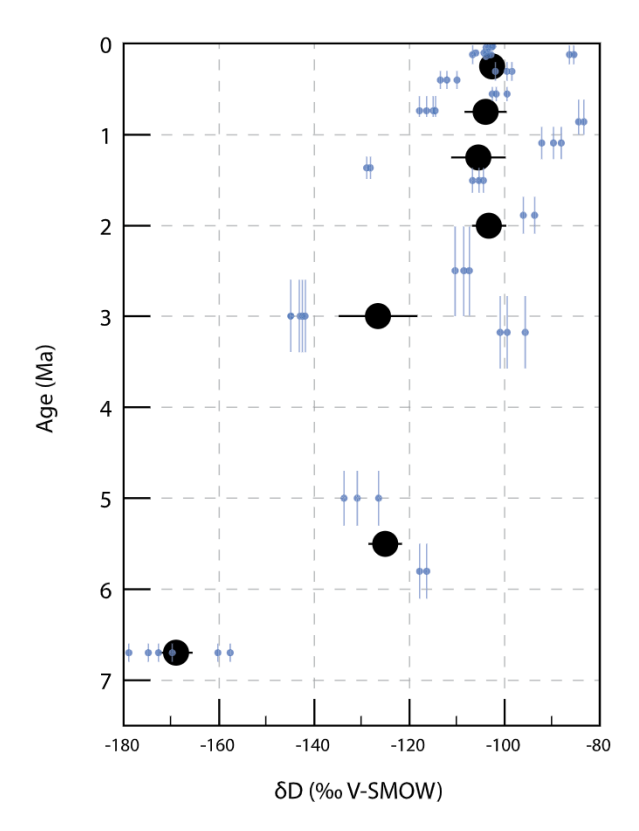


Fig. 5. δD_{clay} results of this study. Larger black circles show the binned population means and population standard error from Table 2. Individual measurements with their age uncertainties are shown as light blue circles (Table S1). Instrumental uncertainty is smaller than symbol size. Age uncertainty is shown from values in Table 2 where available for radiometric ages or estimated from stratigraphic uncertainty. See methods for description of how samples were binned. (For interpretation of the references to color in this figure legend, the reader is referred to the web version of this article.)

Lachniet et al. (2016) data identified on Fig. 3, with the slopes for each individual data set being 6.35, 6.27, 6.47 and 6.88 respectively. The strong divergence of the LMWL slope (6.37) from the GMWL (m=8) suggests evaporative enrichment of surface water in the interior of Alaska (Chipman et al., 2012; Gat, 1996; Yuan et al., 2011).

4.2. Tephra samples

The results of our δD_{clay} data are summarized in Fig. 5 and the corresponding bins are identified in Table 2. These show that our late-Pleistocene δD_{clay} values ($-102.6\,\pm\,1.9\%$) have an offset from modern surface waters north of the Alaska Range (-155to -171%) (Table 1). Lawrence and Taylor (1972, 1971), Savin and Epstein (1970) and Stern et al. (1997) established that the δD (or $\delta^{18}O$) values of clay minerals formed by Holocene weathering form in isotopic equilibrium with local meteoric waters and have an approximate constant offset from the δD (or $\delta^{18}O$) values of local meteoric waters. Several studies have tried to further quantify this offset (e.g. Bird et al., 1992; Chen et al., 1988; Giral-Kacmarcík et al., 1998), but given the uncertainties and assumptions in these estimates of the offset, we do not try to convert our δD_{clav} values to "true" meteoric values. Nonetheless, we did not observe any evidence that our samples did not form in equilibrium with paleo surface waters (e.g. evidence of hydrothermal alteration or secondary mineralization in outcrop or hand sample).

We interpret our δD_{clay} measurements to represent an aggregate signal characterizing paleo-precipitation for the interior of Alaska, leeward of the Alaska, Chugach, Wrangell, and St. Elias mountain ranges (i.e. Chamberlain and Poage, 2000; Blisniuk and

Stern, 2005; Blisniuk et al., 2006). The 7.5–6.5 Ma interval consists of the 6.7 \pm 0.1 Ma Grubstake tephra (Triplehorn et al., 2000), with the $\delta D_{\rm clay}$ measurements (n=6 measurements) showing excellent agreement, establishing the late-Miocene value as $-169.0 \pm 3.4\%$. The next younger bin (6.0–5.0 Ma, n=5) consists of tephras deposited near the top of the Grubstake Formation with a mean $\delta D_{\rm clay}$ value of $-125.1 \pm 3.4\%$ (see Supplementary Material for further details of age control for individual tephra). The 3.5–2.5 Ma bin consists of two tephras that have a mean $\delta D_{\rm clay}$ value of $-126.6 \pm 8.2\%$ (n=8). All younger tephras (<2.5 Ma) and associated younger bins have statistically similar $\delta D_{\rm clay}$ values, which range from $-103.3 \pm 3.5\%$ (n=5), $-105.5 \pm 5.7\%$ (n=8), $-104.0 \pm 4.4\%$ (n=9), and $-102.6 \pm 1.9\%$ (n=16) (Fig. 5, Table 2).

5. Interpretation of the δD_{clay} record

The stable isotope composition of modern precipitation and surface water influenced by multiple equilibrium and kinetic fractionation processes (Hren et al., 2009; Bershaw et al., 2012; Schemmel et al., 2013). Specifically, the isotopic signature of meteoric water from the leeward sides of mountain ranges reflects some combination of four controls: (1) changes in orographic rainout due to topographic development, (2) changing moisture source, transport path, season, and processes of moisture delivery, (3) changes in water vapor recycling through evapotranspiration and (4) long-term climate change. Here we evaluate the relative contributions of these processes to our isotopic signal.

5.1. Topographic development

The largest effect of topography on the isotopic composition of meteoric water is typically the progressive condensation and removal of atmospheric moisture through open-system Rayleigh distillation. As air masses rising over an orographic barrier precipitate moisture (Fig. 2), they preferentially condense H₂¹⁸O and HDO into the liquid and solid phase, leading to decreasing $\delta^{18}O$ and δD values with increasing surface elevation (Blisniuk and Stern, 2005; Dansgaard, 1964; Poage and Chamberlain, 2001). Attributing all of our isotopic signal (>50\% enrichment between \sim 7 and \sim 3 Ma) to this process would imply surface lowering of Alaskan ranges on the order of 2 km (e.g. Poage and Chamberlain, 2001; Rowley and Garzione, 2007) coincident with an acceleration in rates of exhumation and sedimentation (e.g. O'Sullivan and Currie, 1996; White et al., 1997; Sheaf et al., 2003; Ridgway et al., 2007; Fitzgerald et al., 2014; Lease et al., 2016). This scenario is unlikely because of the evidence outlined in Section 2, above. We therefore conclude that the dominant control of surface uplift on the late-Cenozoic δD_{clay} signal of interior Alaska was associated with processes other than open-system Rayleigh distillation of southerly moisture alone.

5.2. Changes in moisture delivery

Surface uplift plays an important role in changing the isotopic composition of precipitation in continental interiors through the direct effect of orographic blocking and steering of vapor transport as well as by changing atmospheric circulation patterns and mixing states between multiple moisture sources to a given basin (e.g. Ehlers and Poulsen, 2009; Poulsen et al., 2010; Feng et al., 2013). Model simulations of the western U.S. have shown that isotopic enrichment of leeside precipitation can occur due to air parcel blocking by and flow around topography (Galewsky, 2009; Lechler and Galewsky, 2013).

Season of moisture delivery can also influence the isotopic signal. The Aleutian Low and associated North Pacific storm track

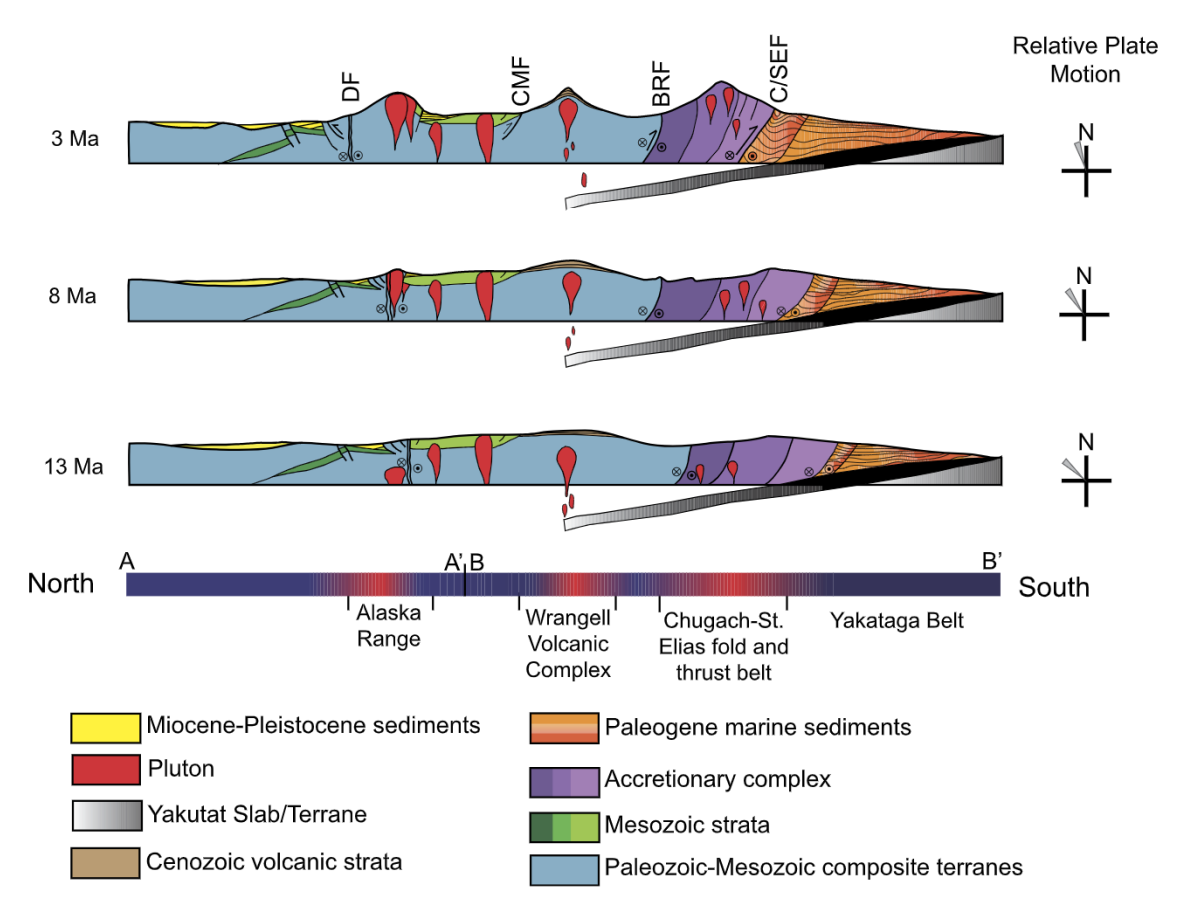


Fig. 6. Conceptual model of increased growth in topography and surface elevations since the Pliocene. This schematic cross sections of generalized geology of Alaska through the late Cenozoic, encompasses the two transects shown in pink lines in Fig. 3. Cross sections were synthesized and re-drawn after: Little and Naeser (1989), Pavlis et al. (2012), Ridgway et al. (2007), Trop and Ridgway (2007).

primarily affect winter-season precipitation, which is more depleted in δD than summer-season precipitation (Fig. S1) and dominates the annual signal on the windward side of the Alaskan ranges (Figs. S2, S3). In contrast, annual precipitation in the interior of Alaska is significantly less than on the windward side of the Alaskan ranges (Fig. 2), and largely falls during the summer (Figs. S2, S3) with more enriched δD values (Fig. S1). From these relationships, we suggest that prior to uplift, the interior of Alaska received a greater amount of winter-season low- δD precipitation as compared to the relatively small amount of summer-season precipitation with high δD values that it receives today, with intervening uplift contributing to the enrichment signal in our δD record.

5.3. Changes in evapotranspiration

Palynological records from the interior of Alaska document an increase in continentality and aridity after \sim 7 Ma, which White et al. (1997) attributed to latest Miocene–Pleistocene uplift of the Alaska and St. Elias ranges. Enhanced continentality and associated increased evaporation can strongly affect the isotopic composition of meteoric water (Bershaw et al., 2012; Chamberlain et al., 2014; Feng et al., 2016; Gat, 1996; Mix et al., 2013; Yuan et al., 2011). In particular, several studies of isotopic transects of meteoric water have interpreted large increases in δD and $\delta^{18}O$ from continental interiors as recording increasingly arid leeward conditions and associated evaporative enrichment of surface waters in response to surface uplift (e.g. Feng et al., 2013; Pingel et al., 2014; Fiorella et al., 2015).

The Tibetan Plateau provides an excellent example of isotopic enrichment due to changes in evapotranspiration. In a south-tonorth transect of the Tibetan plateau, an isotopic depletion signal was observed in transects crossing from the windward to the leeward side of the Himalayan crest, followed by a strong δD enrichment signal ($\sim 60\%$) moving northward into the Tibetan plateau (Bershaw et al., 2012; Hren et al., 2009). Hren et al. (2009) argued that this enrichment was caused by the progressive mixing of moisture sources from the north and west, whereas Bershaw et al. (2012) suggested that evaporation played a primary role in modifying the isotopic signal across the plateau. Caves et al. (2014, 2017) suggested both were important.

Our record of δD enrichment is thus consistent with palynological evidence for aridification of interior Alaska after ~ 7 Ma (White et al., 1997). While we cannot quantify the proportion of our observed signal caused by surface uplift-driven changes in aridity, evaporation and increased aridity have been interpreted as inducing stable-isotope enrichments comparable to those in our δD record not only from closed-basin lakes (e.g. Menking et al., 1997), but also in simulations for areas leeward of mountain ranges (e.g. Feng et al., 2016).

5.4. Late Neogene cooling

Geochemical proxy records suggest that northeastern Pacific sea surface temperatures were $\sim 10\,^{\circ}\text{C}$ warmer than present $\sim 12\,$ Ma, and subsequently cooled to near-modern values by $\sim 6\,$ Ma, with $\sim 7\,^{\circ}\text{C}$ of that cooling occurring after $\sim 7.5\,$ Ma (Herbert et al., 2016). Temperature reconstructions from pollen assemblages in central Alaska suggest a similar degree of cooling, with estimated mean annual temperatures of $10-12\,^{\circ}\text{C}$ during the middle Miocene and $2-3\,^{\circ}\text{C}$ during the Pliocene (Ager, 2007; Ager et al., 1994; White et al., 1997). Assuming a simple Rayleigh-type relationship of 6% per $^{\circ}\text{C}$ observed in high-latitude precipitation

(Dansgaard, 1964; Jouzel et al., 2007), this late Neogene cooling would have caused a significant depletion in δD , suggesting an even larger enrichment signal in central Alaska from surface uplift and its associated effects on moisture transport and regional climate than recorded by our δD_{clav} values.

6. Conclusions

We developed an authigenic δD_{clav} record from the interior of Alaska to constrain the timing of increased late-Cenozoic lateral and vertical surface uplift extent of coastal (St. Elias, Chugach) and interior (Wrangell, Alaska) mountain ranges and its association with increased rates of exhumation and rock uplift beginning \sim 6 Ma. Our δ D record shows a significant (>50%) enrichment between \sim 6- \sim 7 Ma and \sim 2- \sim 3 Ma. Although the timing of this enrichment is consistent with the timing for increased exhumation and rock uplift, the signal would suggest surface lowering if interpreted solely as an orographic control on air masses crossing the Alaskan ranges to the interior. Thermochronologic and sedimentologic evidence for an acceleration in exhumation and rock uplift during this time makes this scenario unlikely, particularly since it would then require that this surface lowering be followed by surface uplift to achieve the present elevated topography. We thus conclude that the most parsimonious interpretation of our data is that changes in aridity, moisture source, and seasonality of moisture resulting from surface uplift offset the expected Rayleigh distillation signal to produce the large increase in δD of meteoric water in the Alaskan interior. We hypothesize that prior to an increase in the lateral extent of the southern Alaskan mountain ranges, the interior of Alaska exhibited a more equable and humid climate, and vegetation had a predominantly denser canopy. In a transition phase, surface uplift (Fig. 6) enhanced continentality of the interior, leading to evaporative enrichment of residual surface waters. Orographically forced changes in atmospheric circulation and associated moisture transport and mixing as well as in the seasonality of moisture may also have contributed to more enriched δD values.

Acknowledgements

We gratefully acknowledge the careful editorial handling of EPSL and the advice of the four anonymous reviewers who provided constructive comments, improving the manuscript. Research was supported by the GSA John T. Dillon Alaska Student Research Award to N. Bill, the AAPG Harry and Joy Jamison Graduate Student Research Grant to N. Bill, and the Santa Clara University Sustainability Research Initiative grant to H. Mix and NSF Award #1434656 to J. Benowitz. We thank J. Beget, S. Burgess, M. Coombs, C. Johnson, Z. Maharrey, and K. Wallace for help with fieldwork in Alaska. We also thank J. Caves, S. Hostetler, A. Meigs, A. Reyes, D. Rowley and T. Waldien for discussions related to this project. We would like to extend our gratitude to B. Gillis and J. Westgate for providing auxiliary tephra samples. We also thank P. Blisniuk for support in the Stanford Stable Isotope Biogeochemistry Laboratory and F. Anslow for support with the PRISM climate data.

Appendix A. Supplementary material

Supplementary material related to this article can be found online at https://doi.org/10.1016/j.epsl.2017.11.029.

References

Ager, T.A., 1994. Terrestrial palynological and paleobotanical records of Pliocene age from Alaska and Yukon territory. U.S. Geol. Surv. Open-File Rep. 94 (23), 2–3. Ager, T.A., 2007. Vegetation response to climate change in Alaska: examples from the fossil record. U.S. Geol. Surv. Open-File Rep. 2007 (1096), 1–44.

- Ager, T.A., Matthews, J.V., Yeend, W., 1994. Pliocene terrace gravels of the ancestral Yukon River near Circle, Alaska: palynology, paleobotany, paleoenvironmental reconstruction and regional correlation. Quat. Int. 22–23, 185–206. https://doi.org/10.1016/1040-6182(94)90012-4.
- Benowitz, J.A., Haeussler, P.J., Layer, P.W., O'Sullivan, P.B., Wallace, W.K., Gillis, R.J., 2012. Cenozoic tectono-thermal history of the Tordrillo Mountains, Alaska: Paleocene–Eocene ridge subduction, decreasing relief, and late Neogene faulting. Geochem. Geophys. Geosyst. 13. https://doi.org/10.1029/2011GC003951.
- Benowitz, J.A., Layer, P.W., Armstrong, P., Perry, S.E., Haeussler, P.J., Fitzgerald, P.G., VanLaningham, S., 2011. Spatial variations in focused exhumation along a continental-scale strike-slip fault: the Denali fault of the eastern Alaska Range. Geosphere 7, 455–467. https://doi.org/10.1130/GES00589.1.
- Benowitz, J.A., Layer, P.W., Vanlaningham, S., 2013. Persistent long-term (c. 24 Ma) exhumation in the Eastern Alaska Range constrained by stacked thermochronology. Geol. Soc. (Lond.) Spec. Publ. 378, 225–243. https://doi.org/10.1144/SP378.12.
- Berger, A.L., Spotila, J.A., Chapman, J.B., Pavlis, T.L., Enkelmann, E., Ruppert, N.A., Buscher, J.T., 2008. Architecture, kinematics, and exhumation of a convergent orogenic wedge: a thermochronological investigation of tectonic-climatic interactions within the central St. Elias orogen, Alaska. Earth Planet. Sci. Lett. 270, 13–24. https://doi.org/10.1016/j.epsl.2008.02.034.
- Bershaw, J., Penny, S.M., Garzione, C.N., 2012. Stable isotopes of modern water across the Himalaya and eastern Tibetan Plateau: implications for estimates of paleoelevation and paleoclimate. J. Geophys. Res. 117. https://doi.org/10.1029/2011/D016132.
- Bird, M.I., Longstaffe, F.J., Fyfe, W.S., Bildgen, P., 1992. Oxygen-isotope systematics in a multiphase weathering system in Haiti. Geochim. Cosmochim. Acta 56, 2831–2838. https://doi.org/10.1016/0016-7037(92)90362-M.
- Bischoff, J.L., 1972. A ferroan nontronite from the Red Sea Geothermal system. Clays Clay Miner. 20, 217–223. https://doi.org/10.1346/CCMN.1972.0200406.
- Blisniuk, P., Stern, L., 2005. Stable isotope paleoaltimetry: a critical review. Am. J. Sci. 305, 1033–1074.
- Blisniuk, P.M., Stern, L.A., Chamberlain, C.P., Zeitler, P.K., Ramos, V.A., Sobel, E.R., Haschke, M., Strecker, M.R., Warkus, F., 2006. Links between mountain uplift, climate, and surface processes in the southern Patagonian Andes. In: The Andes. Springer, Berlin, Heidelberg, pp. 429–440.
- Bowen, G.J., 2017. The online isotopes in precipitation calculator, version 3.1 [WWW document]. http://www.waterisotopes.org.
- Brennan, P.R.K., Ridgway, K.D., 2015. Detrital zircon record of Neogene exhumation of the central Alaska Range: a far-field upper plate response to flat-slab subduction, Geol. Soc. Am. Bull. B 31164 (1). https://doi.org/10.1130/B31164.1.
- Bruhn, R.L., Pavlis, T.L., Plafker, G., Serpa, L., 2004. Deformation during terrane accretion in the Saint Elias orogen, Alaska. Bull. Geol. Soc. Am. 116, 771–787. https://doi.org/10.1130/B25182.1.
- Burkett, C.A., Bemis, S.P., Benowitz, J.A., 2015. Along-fault migration of the Mount McKinley restraining bend of the Denali fault defined by late Quaternary fault patterns and seismicity, Denali National Park & Preserve, Alaska, Tectonophysics 693, 489–506, https://doi.org/10.1016/j.tecto.2016.05.009.
- Campani, M., Mulch, A., Kempf, O., Schlunegger, F., Mancktelow, N., 2012. Miocene paleotopography of the Central Alps. Earth Planet. Sci. Lett. 337–338, 174–185. https://doi.org/10.1016/j.epsl.2012.05.017.
- Canavan, R.R., Carrapa, B., Clementz, M.T., Quade, J., DeCelles, P.G., Schoenbohm, L.M., 2014. Early Cenozoic uplift of the Puna Plateau, Central Andes, based on stable isotope paleoaltimetry of hydrated volcanic glass. Geology 42, 447–450. https://doi.org/10.1130/G35239.1.
- Capuano, R.M., 1992. The temperature dependence of hydrogen isotope fractionation between clay minerals and water: evidence from a geopressured system. Geochim. Cosmochim. Acta 56, 2547–2554. https://doi.org/10.1016/0016-7037(92)90208-Z.
- Caves, J.K., Bayshashov, B.U., Zhamangara, A., Ritch, A.J., Ibarra, D.E., Sjostrom, D.J., Mix, H.T., Winnick, M.J., Chamberlain, C.P., 2017. Late miocene uplift of the Tian Shan and Altai and reorganization of central Asia climate. GSA Today 27. https://doi.org/10.1130/GSATG305A.1.
- Caves, J.K., Sjostrom, D.J., Mix, H.T., Winnick, M.J., Chamberlain, C.P., 2014. Aridification of central Asia and uplift of the Altai and Hangay Mountains, Mongolia: stable isotope evidence. Am. J. Sci. 314, 1171–1201. https://doi.org/10.2475/08.2014.01.
- Chamberlain, C., Poage, M., 2000. Reconstructing the paleotopography of mountain belts from the isotopic composition of authigenic minerals. Geology 28, 115–118. https://doi.org/10.1130/0091-7613(2000)28<115:RTPOMB>2.0.CO;2.
- Chamberlain, C.P., Mix, H.T., Mulch, A., Hren, M.T., Kent-Corson, M.L., Davis, S.J., Horton, T.W., Graham, S.A., 2012. The Cenozoic climatic and topographic evolution of the western North American Cordillera. Am. J. Sci. 312, 213–262. https://doi.org/10.2475/02.2012.05.
- Chamberlain, C.P., Poage, M.A., Craw, D., Reynolds, R.C., 1999. Topographic development of the Southern Alps recorded by the isotopic composition of authigenic clay minerals, South Island, New Zealand. Chem. Geol. 155, 279–294. https://doi.org/10.1016/S0009-2541(98)00165-X.
- Chamberlain, C.P., Winnick, M.J., Mix, H.T., Chamberlain, S.D., Maher, K., 2014. The impact of Neogene grassland expansion and aridification on the isotopic com-

- position of continental precipitation. Glob. Biogeochem. Cycles 28, 992–1004. https://doi.org/10.1002/2014GB004822.
- Chase, C., Gregory-Wodzicki, K., Parrish, J.T., DeCelles, P.G., 1998. Topographic history of the Western Cordillera of North America and controls on climate. In: Crowley, Burke (Ed.), Tectonic Boundary Conditions for Climate Reconstructions. In: Oxford Monograph on Geology and Geophysics, vol. 39, pp. 73–99.
- Chen, C.H., Liu, K.K., Shieh, Y.N., 1988. Geochemical and isotopic studies of bauxitization in the Tatun volcanic area, northern Taiwan. Chem. Geol. 68, 41–56. https://doi.org/10.1016/0009-2541(88)90085-X.
- Chipman, M.L., Clegg, B.F., Hu, F.S., 2012. Variation in the moisture regime of northeastern interior Alaska and possible linkages to the Aleutian Low: inferences from a late-Holocene δ^{18} O record. J. Paleolimnol. 48, 69–81. https://doi.org/10.1007/s10933-012-9599-0.
- Craig, H., 1961. Isotopic variations in meteoric waters. Science 133 (3465), 1702–1703. https://doi.org/10.1126/science.133.3465.1702.
- Dansgaard, W., 1964. Stable isotopes in precipitation. Tellus 16, 436–468. https://doi.org/10.3402/tellusa.v16i4.8993.
- Davis, K., Benowitz, J., Roeske, S., 2015. ⁴⁰Ar/³⁹Ar dating of detrital micas from paleo and modern basin deposits, Interior Alaska: Provenance, Paleodrainage history, and constraints on Neogene orogenesis in the Alaska Range. Abstr. Program Geol. Soc. Am. 47, 51.
- Deepthy, R., Balakrishnan, S., 2005. Climatic control on clay mineral formation: evidence from weathering profiles developed on either side of the Western Ghats. J. Earth Syst. Sci. 114, 545–556. https://doi.org/10.1007/BF02702030.
- Delgado, A., Reyes, E., 1996. Oxygen and hydrogen isotope compositions in clay minerals: a potential single-mineral geothermometer. Geochim. Cosmochim. Acta 60, 4285–4289. https://doi.org/10.1016/S0016-7037(96)00260-8.
- Dickson, R.K., 1981. Uranium Mineralization in the Nenana Coal Field, Alaska, in: Short Notes on Alaska Geology. Alaska Division of Geological & Geophysical Surveys Geologic Report 73, pp. 37–42.
- Duk-Rodkin, A., Barendregt, R.W., Froese, D.G., Weber, F., Enkin, R., Rod Smith, I., Zazula, G.D., Waters, P., Klassen, R., 2004. Timing and extent of Plio-Pleistocene glaciations in north-western Canada and east-central Alaska. In: Developments in Quaternary Science, pp. 313–345.
- Ehlers, T.A., Poulsen, C.J., 2009. Influence of Andean uplift on climate and paleoal-timetry estimates. Earth Planet. Sci. Lett. 281, 238–248. https://doi.org/10.1016/j.epsl.2009.02.026.
- England, P., Molnar, P., 1990. Surface uplift, uplift of rocks, and exhumation of rocks. Geology 18, 1173–1177.
- Enkelmann, E., Zeitler, P.K., Garver, J.I., Pavlis, T.L., Hooks, B.P., 2010. The thermochronological record of tectonic and surface process interaction at the Yakutat–North American collision zone in southeast Alaska. Am. J. Sci. 310, 231–260. https://doi.org/10.2475/04.2010.01.
- Eyles, C.H., Eyles, N., Lagoe, M.B., 1991. The Yakataga formation; a late Miocene to Pleistocene record of temperate glacial marine sedimentation in the Gulf of Alaska. In: Anderson, J.B., Ashley, G.M. (Eds.), Glacial Marine Sedimentation: Paleoclimatic Significance. Geological Society of America, Boulder, CO, pp. 159–180.
- Feng, R., Poulsen, C.J., 2016. Refinement of Eocene lapse rates, fossil-leaf altimetry, and North American Cordilleran surface elevation estimates. Earth Planet. Sci. Lett. 436, 130–141. https://doi.org/10.1016/j.epsl.2015.12.022.
- Feng, R., Poulsen, C.J., Werner, M., 2016. Tropical circulation intensification and tectonic extension recorded by Neogene terrestrial δ^{18} O records of the western United States. Geology 44, 971–974. https://doi.org/10.1130/G38212.1.
- Feng, R., Poulsen, C.J., Werner, M., Chamberlain, C.P., Mix, H.T., Mulch, A., 2013. Early Cenozoic evolution of topography, climate, and stable isotopes in precipitation in the North American Cordillera. Am. J. Sci. 313, 613–648. https://doi.org/10.2475/07.2013.01.
- Fiorella, R.P., Poulsen, C.J., Pillco Zolá, R.S., Jeffery, M.L., Ehlers, T.A., 2015. Modern and long-term evaporation of central Andes surface waters suggests paleo archives underestimate Neogene elevations. Earth Planet. Sci. Lett. 432, 59–72. https://doi.org/10.1016/j.epsl.2015.09.045.
- Fitzgerald, P.G., Roeske, S.M., Benowitz, J.A., Riccio, S.J., Perry, S.E., Armstrong, P.A., 2014. Alternating asymmetric topography of the Alaska Range along the strikeslip Denali Fault: strain partitioning and lithospheric control across a terrane suture zone. Tectonics 33, 1519–1533. https://doi.org/10.1002/2013TC003432.
- Fitzgerald, P.G., Sorkhabi, R.B., Redfield, T.F., Stump, E., 1995. Uplift and denudation of the central Alaska Range: a case study in the use of apatite fission track thermochronology to determine absolute uplift parameters. J. Geophys. Res., Solid Earth 100, 20175–20191. https://doi.org/10.1029/95JB02150.
- Fitzgerald, P.G., Stump, E.S., Redfield, T.F., 1993. Late Cenozoic uplift of Denali and its relation to relative plate motion and fault morphology. Science 80 (259), 497–499. https://doi.org/10.1126/science.259.5094.497.
- Froese, D.G., Smith, D.G., Westgate, J.A., Ager, T.A., Preece, S.J., Sandhu, A., Enkin, R.J., Weber, F., 2003. Recurring middle Pleistocene outburst floods in east-central Alaska. Quat. Res. 60, 50–62. https://doi.org/10.1016/S0033-5894(03)00090-5.
- Galewsky, J., 2009. Orographic precipitation isotopic ratios in stratified atmospheric flows: implications for paleoelevation studies. Geology 37, 791–794. https:// doi.org/10.1130/G30008A.1.

- Galewsky, J., Steen-Larsen, H.C., Field, R.D., Worden, J., Risi, C., Schneider, M., 2016. Stable isotopes in atmospheric water vapor and applications to the hydrologic cycle. Rev. Geophys. 54, 1–169. https://doi.org/10.1002/2015RG000512.
- Garzione, C.N., Dettman, D.L., Quade, J., DeCelles, P.G., Butler, R.F., 2000. High times on the Tibetan Plateau: paleoelevation of the Thakkhola graben, Nepal. Geology 28, 339. https://doi.org/10.1130/0091-7613(2000)28<339:HTOTTP>2.0.CO:2.
- Garzione, C.N., Hoke, G.D., Libarkin, J.C., Withers, S., MacFadden, B., Eiler, J., Ghosh, P., Mulch, A., 2008. Rise of the Andes. Science 320, 1304–1307. https://doi.org/10.1126/science.1148615.
- Gat, J.R., 1996. Oxygen and hydrogen isotopes in the hydrologic cycle. Annu. Rev. Earth Planet. Sci. 24, 225–262. https://doi.org/10.1146/annurev.earth.24.1.225.
- Gebelin, A., Mulch, A., Teyssier, C., Jessup, M.J., Law, R.D., Brunel, M., 2013. The Miocene elevation of Mount Everest. Geology 41, 799–802. https://doi.org/ 10.1130/G34331.1.
- Ghosh, P., Garzione, C.N., Eiler, J.M., 2006. Rapid uplift of the Altiplano revealed through ¹³C-¹⁸O bonds in paleosol carbonates. Science 80 (311), 511–515. https://doi.org/10.1126/science.1119365.
- Giral-Kacmarcík, S., Savin, S.M., Nahon, D.B., Girard, J.P., Lucas, Y., Abel, L.J., 1998. Oxygen isotope geochemistry of kaolinite in laterite-forming processes, Manaus, Amazonas, Brazil. Geochim. Cosmochim. Acta 62, 1865–1879. https://doi.org/ 10.1016/S0016-7037(98)00103-3.
- Grimaldi, D.A., Triplehorn, D.M., 2008. Insects from the upper miocene Grubstake formation of Alaska. Am. Mus. Novit. 3612, 1–19. https://doi.org/10.1206/602.1.
- Haeussler, P.J., O'Sullivan, P., Berger, A.L., Spotila, J.A., 2008. Neogene exhumation of the Tordrillo Mountains, Alaska, and correlations with Denali (Mount Mckinley).
 In: Freymueller, J.J., Haeussler, P.J., Wesson, R., Ekstrom, G. (Eds.), Active Tectonics and Seismic Potential of Alaska. AGU Monograph, pp. 269–285.
- Hallet, B., Hunter, L., Bogen, J., 1996. Rates of erosion and sediment evacuation by glaciers: a review of field data and their implications, Glob. Planet. Change 12, 213–235. https://doi.org/10.1016/0921-8181(95)00021-6.
- Herbert, T.D., Lawrence, K.T., Tzanova, A., Peterson, L.C., Caballero-Gill, R., Kelly, C.S., 2016. Late Miocene global cooling and the rise of modern ecosystems. Nat. Geosci. 9, 843–847. https://doi.org/10.1038/ngeo2813.
- Hren, M.T., Bookhagen, B., Blisniuk, P.M., Booth, A.L., Chamberlain, C.P., 2009. δ¹⁸O and δD of streamwaters across the Himalaya and Tibetan Plateau: implications for moisture sources and paleoelevation reconstructions. Earth Planet. Sci. Lett. 288, 20–32. https://doi.org/10.1016/j.epsl.2009.08.041.
- Insel, N., Poulsen, C.J., Ehlers, T.A., Sturm, C., 2012. Response of meteoric $\delta^{18}O$ to surface uplift implications for Cenozoic Andean Plateau growth. Earth Planet. Sci. Lett. 317–318, 262–272. https://doi.org/10.1016/j.epsl.2011.11.039.
- Jouzel, J., Masson-Delmotte, V., Cattani, O., Dreyfus, G., Falourd, S., Hoffmann, G., Minster, B., Nouet, J., Barnola, J.M., Chappellaz, J., Fischer, H., Gallet, J.C., Johnsen, S., Leuenberger, M., Loulergue, L., Luethi, D., Oerter, H., Parrenin, F., Raisbeck, G., Raynaud, D., Schilt, A., Schwander, J., Selmo, E., Souchez, R., Spahni, R., Stauffer, B., Steffensen, J.P., Stenni, B., Stocker, T.F., Tison, J.L., Werner, M., Wolff, E.W., 2007. Orbital and millennial Antarctic climate variability over the past 800,000 years. Science 80 (317), 793–796. https://doi.org/10.1126/science.1141038.
- Kendall, C., Coplen, T.B., 2001. Distribution of oxygen-18 and deuterium in river waters across the United States. Hydrol. Process. 15, 1363–1393. https://doi.org/10.1002/hyp.217.
- Lachniet, M.S., Lawson, D.E., Stephen, H., Sloat, A.R., Patterson, W.P., 2016. Isoscapes of δ^{18} O and δ^{2} H reveal climatic forcings on Alaska and Yukon precipitation. Water Resour. Res. 52, 6575–6586. https://doi.org/10.1002/2016WR019436.
- Lagoe, M.B., Eyles, C.H., Eyles, N., Hale, C., 1993. Timing of late Cenozoic tidewater glaciation in the far North Pacific. Geol. Soc. Am. Bull. 105, 1542–1560. https://doi.org/10.1130/0016-7606.
- Lawrence, J.R., Taylor, H.P., 1971. Deuterium and oxygen-18 correlation: clay minerals and hydroxides in Quaternary soils compared to meteoric waters. Geochim. Cosmochim. Acta 35, 993–1003. https://doi.org/10.1016/0016-7037(71)90017-2.
- Lawrence, J.R., Taylor, H.P., 1972. Hydrogen and oxygen isotope systematics in weathering profiles. Geochim. Cosmochim. Acta 36, 1377–1393. https://doi.org/ 10.1016/0016-7037(72)90068-3.
- Lease, R.O., Haeussler, P.J., O'Sullivan, P., 2016. Changing exhumation patterns during Cenozoic growth and glaciation of the Alaska Range: insights from detrital thermochronology and geochronology. Tectonics 35, 934–955. https://doi.org/10.1002/2015TC004067.
- Lechler, A.R., Galewsky, J., 2013. Refining paleoaltimetry reconstructions of the Sierra Nevada, California, using air parcel trajectories. Geology 41, 259–262. https://doi.org/10.1130/G33553.1.
- Little, T.A., Naeser, C.W., 1989. Tertiary tectonics of the Border Ranges fault system, Chugach Mountains, Alaska: deformation and uplift in a forearc setting. J. Geophys. Res., Solid Earth 94, 4333–4359. https://doi.org/10.1029/JB094iB04p04333.
- McAleer, R.J., Spotila, J.A., Enkelmann, E., Berger, A.L., 2009. Exhumation along the Fairweather fault, southeastern Alaska, based on low-temperature thermochronometry. Tectonics 28, 1–17. https://doi.org/10.1029/2007TC002240.
- Meigs, A., Johnston, S., Garver, J., Spotila, J., 2008. Crustal-scale structural architecture, shortening, and exhumation of an active, eroding orogenic wedge (Chugach/St Elias Range, southern Alaska). Tectonics 27. https://doi.org/10.1029/2007TC002168
- Menking, K.M., Bischoff, J.L., Fitzpatrick, J.A., Burdette, J.W., Rye, R.O., 1997. Climatic/hydrologic oscillations since 155,000 vr B.P. at Owens Lake. California.

- reflected in abundance and stable isotope composition of sediment carbonate. Quat. Res. 48, 58–68. https://doi.org/10.1006/qres.1997.1898.
- Mix, H.T., Chamberlain, C.P., 2014. Stable isotope records of hydrologic change and paleotemperature from smectite in Cenozoic western North America. Geochim. Cosmochim. Acta 141, 532–546. https://doi.org/10.1016/j.gca.2014.07.008.
- Mix, H.T., Ibarra, D.E., Mulch, A., Graham, S.A., Chamberlain, C.P., 2016. A hot and high Eocene Sierra Nevada. Geol. Soc. Am. Bull. 128, 531–542. https://doi.org/ 10.1130/B31294.1.
- Mix, H.T., Mulch, A., Kent-Corson, M.L., Chamberlain, C.P., 2011. Cenozoic migration of topography in the North American Cordillera. Geology 39, 87–90. https:// doi.org/10.1130/G31450.1.
- Mix, H.T., Winnick, M.J., Mulch, A., Chamberlain, C.P., 2013. Grassland expansion as an instrument of hydrologic change in Neogene western North America. Earth Planet. Sci. Lett. 377–378, 73–83. https://doi.org/10.1016/j.epsl.2013.07.032.
- Mulch, A., 2016. Stable isotope paleoaltimetry and the evolution of land-scapes and life. Earth Planet. Sci. Lett. 433, 180–191. https://doi.org/10.1016/j.epsl.2015.10.034.
- Mulch, A., Chamberlain, C.P., 2007. Stable isotope paleoaltimetry in orogenic belts: the silicate record in surface and crustal geological archives. Rev. Mineral. Geochem. 66, 89–118. https://doi.org/10.2138/rmg.2007.66.4.
- Mulch, A., Uba, C.E., Strecker, M.R., Schoenberg, R., Chamberlain, C.P., 2010. Late miocene climate variability and surface elevation in the central Andes. Earth Planet. Sci. Lett. 290, 173–182. https://doi.org/10.1016/j.epsl.2009.12.019.
- Naeser, N.D., Westgate, J.A., Hughes, O.L., Péwé, T.L., 1982. Fission-track ages of late Cenozoic distal tephra beds in the Yukon Territory and Alaska. Can. J. Earth Sci. 19, 2167–2178. https://doi.org/10.1139/e82-191.
- O'Sullivan, P., Plafker, G., Murphy, J.M., 1997. Apatite fission-track thermotectonic history of crystalline rocks in the northern Saint Elias Mountains, Alaska. In: Geologic Studies in Alaska by the U.S. Geological Survey. USGS, pp. 283–294.
- O'Sullivan, P.B., Currie, L.D., 1996. Thermotectonic history of Mt Logan, Yukon Territory, Canada: implications of multiple episodes of middle to late Cenozoic denudation. Earth Planet. Sci. Lett. 144, 251–261. https://doi.org/10.1016/0012-821X(96)00161-6.
- Pavlis, T.L., Chapman, J.B., Bruhn, R.L., Ridgway, K., Worthington, L.L., Gulick, S.P.S., Spotila, J., 2012. Structure of the actively deforming fold-thrust belt of the St. Elias orogen with implications for glacial exhumation and three-dimensional tectonic processes. Geosphere 8, 991–1019. https://doi.org/10.1130/GES00753.1.
- Pavlis, T.L., Hamburger, M.W., Pavlis, G.L., 1997. Erosional processes as a control on the structural evolution of an actively deforming fold and thrust belt: an example from the Pamir-Tien Shan region, central Asia. Tectonics 16, 810. https:// doi.org/10.1029/97TC01414.
- Pavlis, T.L., Picornell, C., Serpa, L., Bruhn, R.L., Plafker, G., 2004. Tectonic processes during oblique collision: insights from the St. Elias orogen, northern North American Cordillera. Tectonics 23, 1–15. https://doi.org/10.1029/2003TC001557.
- Péwé, T.L., Westgate, J.A., Preece, S.J., Brown, P.M., Leavitt, S.W., 2009. Late Pliocene Dawson Cut Forest Bed and new tephrochronological findings in the Gold Hill Loess, east-central Alaska. Geol. Soc. Am. Bull. 121, 294–320. https://doi.org/ 10.1130/B26323.1.
- Pingel, H., Alonso, R.N., Mulch, A., Rohrmann, A., Sudo, M., Strecker, M.R., 2014.
 Pliocene orographic barrier uplift in the southern central Andes. Geology 42, 691–694. https://doi.org/10.1130/G35538.1.
- Plafker, G., Moore, J.C., Winkler, G.R., 1994. Geology of the southern Alaska margin. In: Plafker, G., Berg, H.C. (Eds.), The Geology of Alaska. The Geological Society of America, pp. 389–448.
- Plafker, G., Naeser, C.W., Zimmermann, R.A., Lull, J.S., Hudson, T., 1992. Cenozoic uplift history of the Mount McKinley area in the central Alaska Range based on fission-track dating. In: Geologic Studies in Alaska by the U.S. Geological Survey. USGS, pp. 202–212.
- Poage, M.A., Chamberlain, C.P., 2001. Empirical relationships between elevation and the stable isotope composition of precipitation and surface waters; considerations for studies of paleoelevation change. Am. J. Sci. 301, 1–15. https://doi.org/ 10.2475/ajs.301.1.1.
- Poage, M.A., Chamberlain, C.P., 2002. Stable isotopic evidence for a Pre-Middle Miocene rain shadow in the western Basin and Range: implications for the paleotopography of the Sierra Nevada. Tectonics 21, 16-1-16-10. https://doi.org/ 10.1029/2001TC001303.
- Poulsen, C.J., Ehlers, T.A., Insel, N., 2010. Onset of convective rainfall during gradual late Miocene rise of the Central Andes. Science 80 (328), 490–493. https://doi.org/10.1126/science.1185078.
- Preece, S.J., Westgate, J.A., Froese, D.G., Perkins, W.T., 2011. A catalogue of late Cenozoic tephra beds in the Klondike goldfields and adjacent areas, Yukon. Can. J. Earth Sci. 1418, 1386–1418. https://doi.org/10.1139/E10-110.
- Riccio, S.J., Fitzgerald, P.G., Benowitz, J.A., Roeske, S.M., 2014. The role of thrust faulting in the formation of the eastern Alaska Range: thermochronological constraints from the Sustina Glacier Thrust Fault region of the intracontinental strike-slip Denali Fault system. Tectonics 33, 2195–2217. https:// doi.org/10.1002/2014TC003646.
- Ridgway, K.D., Thoms, E.E., Layer, P.W., Lesh, M.E., White, J.M., Smith, S.V., 2007. Neogene transpressional foreland basin development on the north side of the central Alaska Range, Usibelli Group and Nenana Gravel, Tanana basin. In: Spe-

- cial Paper 431: Tectonic Growth of a Collisional Continental Margin: Crustal Evolution of Southern Alaska. Geological Society of America, pp. 507–547.
- Rowley, D.B., Currie, B.S., 2006. Palaeo-altimetry of the late Eocene to Miocene Lunpola Basin, central Tibet. Nature 439, 677–681. https://doi.org/10.1038/ nature04506.
- Rowley, D.B., Garzione, C.N., 2007. Stable isotope-based paleoaltimetry. Annu. Rev. Earth Planet. Sci. 35, 463–508. https://doi.org/10.1146/annurev.earth. 35.031306140155.
- Rowley, D.B., Pierrehumbert, R.T., Currie, B.S., 2001. A new approach to stable isotope-based paleoaltimetry: implications for paleoaltimetry and paleohypsometry of the High Himalaya since the Late Miocene. Earth Planet. Sci. Lett. 188, 253–268. https://doi.org/10.1016/S0012-821X(01)00324-7.
- Ryan, W.B.F., Carbotte, S.M., Coplan, J.O., O'Hara, S., Melkonian, A., Arko, R., Weissel, R.A., Ferrini, V., Goodwillie, A., Nitsche, F., Bonczkowski, J., Zemsky, R., 2009. Global multi-resolution topography synthesis. Geochem. Geophys. Geosyst. 10, 1–9. https://doi.org/10.1029/2008GC002332.
- Savage, J.C., Plafker, G., 1991. Tide gage measurements of uplift along the south coast of Alaska. J. Geophys. Res., Solid Earth 96, 4325–4335. https://doi.org/ 10.1029/90JB02540.
- Savin, S.M., Epstein, S., 1970. The oxygen and hydrogen isotope geochemistry of clay minerals. Geochim. Cosmochim. Acta 34, 25–42.
- Savin, S.M., Lee, M., 1988. Hydrous phyllosilicates. In: Bailey, S.W. (Ed.), Hydrous Phyllosilicates: Reviews in Mineralogy, vol. 19, pp. 189–223.
- Schemmel, F., Mikes, T., Rojay, B., Mulch, A., 2013. The impact of topography on isotopes in precipitation across the Central Anatolian Plateau (Turkey). Am. J. Sci. 313, 61–80. https://doi.org/10.2475/02.2013.01.
- Sharp, Z.D., 1990. A laser-based microanalytical method for the in situ determination of oxygen isotope ratios of silicates and oxides, Geochim. Cosmochim. Acta 54, 1353–1357. https://doi.org/10.1016/0016-7037(90)90160-M.
- Sheaf, M.A., Serpa, L., Pavlis, T.L., 2003. Exhumation rates in the St. Elias Mountains, Alaska. Tectonophysics 367, 1–11. https://doi.org/10.1016/S0040-1951(03)00124-0.
- Sjostrom, D.J., Hren, M.T., Horton, T.W., Waldbauer, J.R., Chamberlain, C.P., 2006. Stable isotopic evidence for a pre-late Miocene elevation gradient in the Great Plains-Rocky Mountain region, USA. In: Willett, S.D., Hovius, N., Brandon, M.T., Fisher, D.M. (Eds.), Tectonics, Climate, and Landscape Evolution. In: Geological Society of America Special Papers, pp. 309–319.
- Skulski, T., Francis, D., Ludden, J., 1992. Volcanism in an arc-transform transition zone: the stratigraphy of the St. Clare Creek volcanic field, Wrangell volcanic belt, Yukon, Canada. Can. J. Earth Sci. 29, 446–461. https://doi.org/10.1139/ e92-039.
- Souther, J.G., Stanciu, C., 1975. Operation Saint Elias, Yukon Territory: Tertiary volcanic rocks. In: Report of Activities, Part A. Geological Survey of Canada, pp. 63–70.
- Stern, L.A., Blisniuk, P.M., 2002. Stable isotope composition of precipitation across the southern Patagonian Andes. J. Geophys. Res., Atmos. 107. https://doi.org/ 10.1029/2002JD002509p.
- Stern, L., Chamberlain, C.P., Reynolds, R.C., Johnson, G.D., 1997. Oxygen isotope evidence of climate change from pedogenic clay minerals in the Himalayan molasse. Geochim. Cosmochim. Acta 61, 731–744.
- Tabor, N.J., Montañez, I.P., 2005. Oxygen and hydrogen isotope compositions of Permian pedogenic phyllosilicates: development of modern surface domain arrays and implications for paleotemperature reconstructions. Palaeogeogr. Palaeoclimatol. Palaeoecol. 223, 127–146. https://doi.org/10.1016/j.palaeo.2005.04.009.
- Takeuchi, A., Larson, P.B., 2005. Oxygen isotope evidence for the late Cenozoic development of an orographic rain shadow in eastern Washington, USA. Geology 33, 313. https://doi.org/10.1130/G21335.1.
- Triplehorn, D.M., 1976. Clay Mineralogy and Petrology of the Coal-Bearing Group Near Healy, Alaska. Alaska Division of Geological & Geophysical Surveys Geologic Report 52
- Triplehorn, D.M., Drake, J., Layer, P.W., 2000. Preliminary ⁴⁰ArJ³⁹Ar Ages from Two Units in the Usibelli Group, Healy, Alaska. Short Notes Alaska Geol. 1999: Alaska Div. Geol. Geophys. Surv. PR 119, pp. 117–128.
- Trop, J.M., Ridgway, K.D., 2007. Mesozoic and Cenozoic tectonic growth of southern Alaska: a sedimentary basin perspective. In: Ridgway, K.D., Trop, J.M., Glen, J.M.G., O'Neill, J.M. (Eds.), Tectonic Growth of a Collisional Margin: Crustal Evolution of Southern Alaska. Geological Society of America Special Paper. pp. 55–94.
- Wahrhaftig, C., Wolfe, J.A., Leopold, E.B., Lanphere, M.A., 1969. The coal-bearing group in the Nenana Coal Field, Alaska, U.S. Geol. Surv. Bull. 1274–D, 1–30.
- Westgate, J.A., Stemper, B.A., Péwé, T.L., 1990. A 3 m.y. record of Pliocene–Pleistocene loess in interior Alaska. Geology 18, 858. https://doi.org/10.1130/0091-7613(1990)018<0858
- White, J.M., Ager, T.A., Adam, D.P., Leopold, E.B., Liu, G., Jetté, H., Schweger, C.E., 1997. An 18 million year record of vegetation and climate change in northwestern Canada and Alaska: tectonic and global climatic correlates. Palaeogeogr. Palaeoclimatol. Palaeoecol. 130, 293–306. https://doi.org/10.1016/S0031-0182(96)00146-0.
- Wolfe, J.A., Forest, C.E., Molnar, P., 1998. Paleobotanical evidence of Eocene and Oligocene paleoaltitudes in midlatitude western North America. Geol. Soc. Am. Bull. 110, 664–678. https://doi.org/10.1130/0016-7606(1998)110 <0664:PEOEAO>2.3.CO;2.

Yapp, C.J., 2008. ¹⁸O/¹⁶O and D/H in goethite from a North American oxisol of the early Eocene climatic optimum. Geochim. Cosmochim. Acta 72, 5838–5851. https://doi.org/10.1016/j.gca.2008.09.002. Yuan, F., Sheng, Y., Yao, T., Fan, C., Li, J., Zhao, H., Lei, Y., 2011. Evaporative enrichment of oxygen-18 and deuterium in lake waters on the Tibetan Plateau. J. Paleolimnol. 46, 291–307. https://doi.org/10.1007/s10933-011-9540-y.